Environ Monit Assess (2020) 192: 716
https://doi.org/10.1007/s10661-020-08689-1

Summer season sea surface temperature changes in the Aegean Sea based on 30 years (1989–2019) of Landsat thermal infrared data

Tuncay Kuleli · **Seyma Bayazit**

Received: 26 June 2020 / Accepted: 15 October 2020 / Published online: 20 October 2020

Abstract In this research, sea surface temperature (SST) variability for the summer season in the Aegean Sea was analysed over a period of 30 years by using the Landsat thermal infrared bands. A total of 88 Landsat 5, 7, and 8 thermal infrared satellite images from June, July, and August were used for each year from 1989 to 2019. To estimate SST from the thermal infrared band data, thermal infrared sensor at-sensor spectral radiance, and thermal infrared sensor top-of-atmosphere brightness temperatures were used. SST pixel values were extracted from thermal images for the 3-month summer season of each year. In order to validate the findings, regression analysis was performed between the Mediterranean Sea Ultra High Resolution SST L4 data and Landsat data for the 2008–2019 period. Regression constant *R*-squared values were found to be 0.9672 for June, 0.9550 for July, 0.9634 for August, and 0.9634 for all summer seasons. It was calculated that the minimum value of the average SST was 18.44 ± 2.87 °C in 1992, and the maximum value of the average SST was 23.45 ± 0.70 °C in 2018. According to the Landsat data, over the past 30 years, the annual average SST changes were estimated to be 0.11 °C, and the total changes of average SST were estimated to be 3.19 ± 1.26 °C. As a result of the analysis and the validation, we can see that there is a rising trend in sea surface temperature in the Aegean Sea. However, it is difficult to determine whether this upward trend is related to global climate change.

Keywords Aegean Sea · GHRSST · Landsat TIR · Sea surface temperature · SST

T. Kuleli (✉)
Bodrum Maritime Vocational School, Mugla Sıtkı Kocman University, 48420 Bodrum/Muğla, Ortakent, Turkey
e-mail: tuncaykuleli@mu.edu.tr

S. Bayazit
Maritime Faculty, Bandirma Onyedi Eylul University, 10200 Bandirma/Balikesir, Turkey
e-mail: sbayazit@bandirma.edu.tr

Introduction

Sea surface temperature (SST) is a major parameter and primary factor associated with physical ocean-coastal dynamics, atmospheric model simulations, and marine ecosystem functions and is also important for marine organisms (Bertram et al. 2001; Uncles and Stephens 2001; Fisher and Mustard 2004; Laffoley and Baxter 2016). SST changes are a critical issue because the oceans cover more than two-thirds of the Earth's surface, and researchers measure and record SST to understand how the oceans interact with the atmosphere (Costello et al. 2015). For these reasons, the measurement of SST plays an important role in many fields of scientific research. Researchers use several tools to measure SST such as buoys, ships, ocean reference stations, marine telemetry, and temperature sensors on satellites. In situ measurements are highly accurate but have a limited spatial extent. Satellite-based thermal infrared (TIR) remote sensing (RS) is a useful technique for monitoring changes in SST over wide spatial extents (Schott 1982; Schott et al. 2001; Ritchie and Cooper

2001; Xing et al. 2006). RS has made it possible to perform long-term monitoring of global SST. According to long-term observations, while SST varies from region to region, it tends to increase at a global scale (Hansen et al. 2010; Laffoley and Baxter 2016; Schmidt and Arndt 2018). Research has been conducted in different parts of the world for many years to identify and understand regional changes in SST by using TIR-RS. Examples of such research include the creation of a temperature profile of the Alfeios River Basin in Greece (Nikolakopoulos et al. 2003); analysis of the sea surface climate of southern New England with Landsat thermal infrared data (Fisher and Mustard 2004); in situ validation of Tropical Rainfall Measuring Mission microwave sea surface temperatures in the tropical Atlantic (Gentemann et al. 2004); use of Landsat-5 and Landsat-7 data to retrieve SST from the coastal waters of Daya Bay, Hong Kong (Xing et al. 2006); construction of sea surface temperature trends and future scenarios for the Mediterranean Sea (Shaltout and Anders Omstedt 2014); determination of high-resolution satellite turbidity and sea surface temperature in the northern Adriatic Sea (Brando et al. 2015); retrieval of SST over Poteran Island in Indonesia with a Landsat 8 TIRS image (Syariza et al. 2015); prediction of historical and future trends in SST in the Indo-Pacific Region (Khalil et al. 2016); and analysis of trends and spatial patterns of SST in the Mediterranean (Pastor et al. 2017).

Various studies have been conducted on SST in the Aegean Sea, which is an important northeastern part of the Mediterranean Sea (Vlahakis and Pollatou 1993; Poulos et al. 1997; Bozkurt and Sen 2011; Skliris et al. 2011; Topouzelis et al. 2012; Turuncoglu 2015). However, research on changes in the near-shore and the gulf SST in the Aegean Sea is lacking.

The main objective of this study is to research and analyse whether there is any change in SST in the research area over a 30-year period. To achieve this goal, summer season (June, July, and August) SST changes in the Aegean Sea were analysed for a 1989–2019 period by using Landsat thermal infrared bands. A total of 88 Landsat 5, 7, and 8 TIR satellite images from June, July, and August were used for each year from 1989 to 2019. To estimate the SST from the TIR band data, thermal infrared sensor (TIRS) at-sensor spectral radiance, and TIRS top-of-atmosphere brightness temperatures were used. Calculated SST values during the same months in different years were analysed for the entire research area.

Research area

The research area is located in the Aegean Sea, including the Gulf of Kusadasi; the Gulf of Gulluk; and the Gulfs of Gokova, Marmaris, and Bodrum (Fig. 1). Along with many large and small islands, there are many bays and gulfs due to the indented coastline in the research area.

Data and methods

Many satellites have various sensor, spatial, temporal, and radiometric resolutions and TIR instruments for measuring SST, for instance, AVHRR, POES, ATSR, ERS-2, GOES, MODIS, EOS Terra-Aqua, and Landsat TM. The usefulness of thermal infrared data from remote-sensing platforms mostly depends on the quality of the data in terms of spatial/temporal/radiometric resolution, cloudiness, and gaps as well as other aspects such as processing, cost, and ease of access. In this research, TIR satellite data from Landsat 5, 7, and 8 Thermal Infrared Sensor (OLI-TRS) for the years between 1989 and 2019 were downloaded from the US Geological Survey (USGS) website (http://earthexplorer.usgs.gov) free of cost. A total of 88 Landsat TIR images acquired during the summer season (June, July, and August) from 1989 to 2019 were used for the analysis (Table 1).

It is very difficult to find satellite images taken the same month and day for different years of a 30-year period. For this reason, images from the closest day possible were chosen for each month in this analysis. Day differences between images of the same month compared to the previous year are shown in Table 2.

The research area was divided into 1326 vector-polygon grids, and each grid is 2 km^2. The research area was divided into grids for four reasons: there are (a) many large and small islands (land area); (b) cloudy areas in some images; (c) areas with unknown objects; and (d) areas with incorrect data from satellite sensors (Fig. 2). Thus, the island areas, missing data, and cloudy areas—although not too many—were easily eliminated.

Missing grids for some years, due to errors and cloud effects, are given in Table 3. For example, because of the cloud effect, there are 75 missing grids in June 1989, which is 5.7% of the total research area.

To estimate SST from the thermal band data, the digital number (DN) of bands was converted to

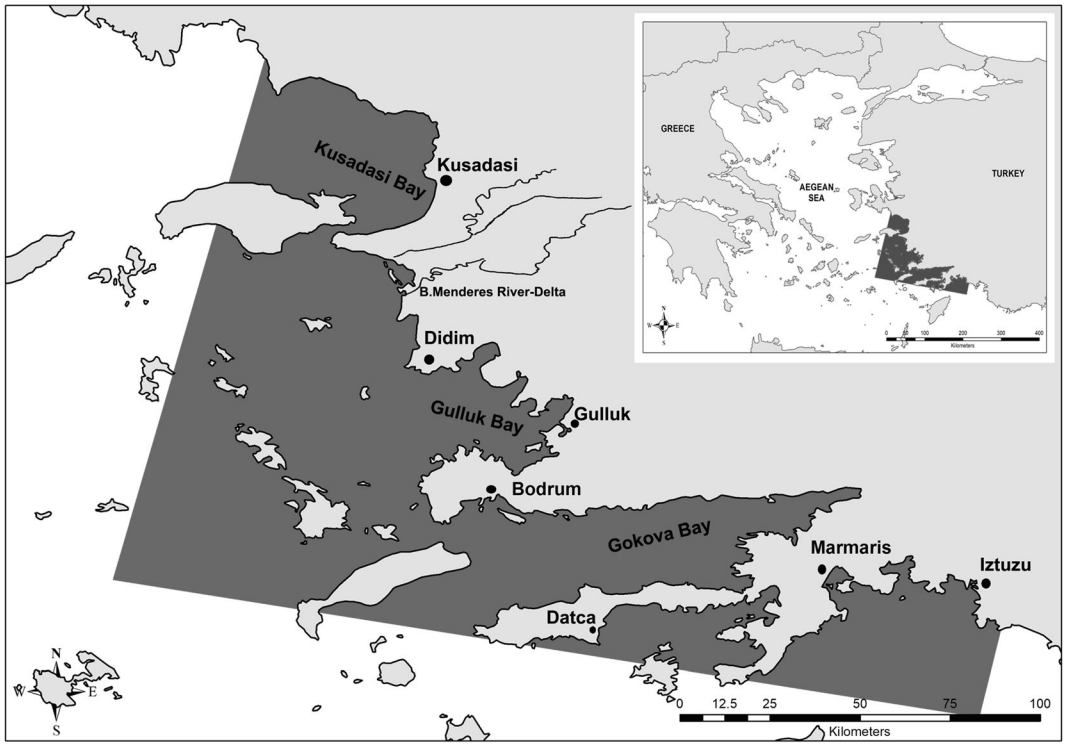

Fig. 1 Research area: The research area is located in the Aegean Sea, shown in dark grey on the map

brightness temperature by using the metadata and the Semi-Automatic Classification Plugin (Luca 2016) for QGIS software. Landsat 5 and 8 provide metadata for the bands such as the thermal constant and the rescaling factor (gain and bias) values (Table 4).

The first step was to convert the DN value of sensors to spectral radiance. The equations used were as follows (Chander et al. 2007; Chander et al. 2009; USGS 2016):

$$L_\lambda = L_{\min(\lambda)} + \left(\frac{L_{\max(\lambda)} - L_{\min(\lambda)}}{Q_{\text{calmax}} - Q_{\text{calmin}}}\right).(Q_{\text{cal}} - Q_{\text{calmin}}) \quad (1)$$

or

$$L_\lambda = G_{\text{rescale}}.Q_{\text{cal}} + B_{\text{rescale}} \quad (2)$$

where

$$G_{\text{rescale}} = \frac{L_{\max(\lambda)} - L_{\min(\lambda)}}{Q_{\text{calmax}} - Q_{\text{calmin}}} \quad (3)$$

$$B_{\text{rescale}} = L_{\min(\lambda)} - \left(\frac{L_{\max(\lambda)} - L_{\min(\lambda)}}{Q_{\text{calmax}} - Q_{\text{calmin}}}\right).(Q_{\text{calmin}}) \quad (4)$$

where L_λ = spectral radiance at the sensor's aperture [W/(m^2 sr μm)]; Q_{cal} = quantized calibrated pixel value (DN); Q_{calmin} = minimum quantized calibrated pixel value corresponding to $L_{(\min\lambda)}$ [DN]; Q_{calmax} = maximum quantized calibrated pixel value corresponding to $L_{(\max\lambda)}$ [DN]; $L_{(\min\lambda)}$ = at-sensor spectral radiance scaled to Q_{calmin} [W/(m^2 sr μm)]; $L_{(\max\lambda)}$ = at-sensor spectral radiance scaled to Q_{calmax} [W/(m^2 sr μm)]; G_{rescale} = band-specific rescaling gain factor [(W/(m^2 sr μm))/DN]; and B_{rescale} = band-specific rescaling bias factor [W/(m^2 sr μm)].

The second step was to convert the at-sensor spectral radiance to the effective at-sensor brightness temperature. The conversion equation used was as follows (Chander et al. 2007; Chander et al. 2009; USGS 2016):

$$T = \frac{K_2}{\ln\left(\frac{K1}{L_\lambda} + 1\right)} \quad (5)$$

where T = effective at-sensor brightness temperature (K); K_2 = calibration constant 2 (K); K_1 = calibration constant 1 [W/(m^2 sr μm)]; $L\lambda$ = spectral radiance at the sensor's aperture [W/(m^2 sr μm)]; ln = natural logarithm.

Table 1 List of the Landsat images. There are a total of 93 Landsat images of the research area. However, 88 images were used for analysis due to images not found in the archive. Missing images are shown as (*)

June		July		August	
Year-day	LANDSAT-band	Year-day	LANDSAT-band	Year-day	LANDSAT-band
1989-10	LANDSAT_5-B6	1989-28	LANDSAT_5-B6	1989-13	LANDSAT_5-B6
1990-13	LANDSAT_5-B6	1990-31	LANDSAT_5-B6	1990-08	LANDSAT_5-B6
1991-16	LANDSAT_5-B6	1991-18	LANDSAT_5-B6	1991-19	LANDSAT_5-B6
1992-18	LANDSAT_5-B6	1992-04	LANDSAT_5-B6	1992-21	LANDSAT_5-B6
1993-21	LANDSAT_5-B6	1993-23	LANDSAT_5-B6	1993-24	LANDSAT_5-B6
1994-24	LANDSAT_5-B6	1994-10	LANDSAT_5-B6	1994-11	LANDSAT_5-B6
1995-27	LANDSAT_5-B6	199513	LANDSAT_5-B6	1995-14	LANDSAT_5-B6
1996-29	LANDSAT_5-B6	1996-15	LANDSAT_5-B6	1996-16	LANDSAT_5-B6
1997-16	LANDSAT_5-B6	1997-02	LANDSAT_5-B6	1997-19	LANDSAT_5-B6
1998-19	LANDSAT_5-B6	1998-21	LANDSAT_5-B6	1998-06	LANDSAT_5-B6
1999-22	LANDSAT_5-B6	1999-24	LANDSAT_5-B6	1999-17	LANDSAT_7-B6_1
2000-24	LANDSAT_5-B6	2000-26	LANDSAT_5-B6	2000-19	LANDSAT_7-B6_1
2001-27	LANDSAT_5-B6	2001-05	LANDSAT_7-B6_1	2001-06	LANDSAT_7-B6_1
2002-30	LANDSAT_5-B6	2002-24	LANDSAT_7-B6_1	2002-09	LANDSAT_7-B6_1
2003*	N/A	2003-03	LANDSAT_5-B6	2003-20	LANDSAT_5-B6
2004-03	LANDSAT_5-B6	2004-21	LANDSAT_5-B6	2004-22	LANDSAT_5-B6
2005-22	LANDSAT_5-B6	2005-24	LANDSAT_5-B6	2005-25	LANDSAT_5-B6
2006-09	LANDSAT_5-B6	2006-27	LANDSAT_5-B6	2006-28x	LANDSAT_5-B6
2007-12	LANDSAT_5-B6	2007-30	LANDSAT_5-B6	2007-15	LANDSAT_5-B6
2008-30	LANDSAT_5-B6	2008*	N/A	2008-17	LANDSAT_5-B6
2009-17	LANDSAT_5-B6	2009-19	LANDSAT_5-B6	2009-20	LANDSAT_5-B6
2010-04	LANDSAT_5-B6	2010-06	LANDSAT_5-B6	2010-23	LANDSAT_5-B6
2011-23	LANDSAT_5-B6	2011-09	LANDSAT_5-B6	2011-10	LANDSAT_5-B6
2012*	N/A	2012*	N/A	2012*	N/A
2013-28	LANDSAT_8-B10	2013-30	LANDSAT_8-B10	2013-15	LANDSAT_8-B10
2014-15	LANDSAT_8-B10	2014-01	LANDSAT_8-B10	2014-18	LANDSAT_8-B10
2015-18	LANDSAT_8-B10	2015-20	LANDSAT_8-B10	2015-21	LANDSAT_8-B10
2016-20	LANDSAT_8-B10	2016-06	LANDSAT_8-B10	2016-07	LANDSAT_8-B10
2017-23	LANDSAT_8-B10	2017-09	LANDSAT_8-B10	2017-26	LANDSAT_8-B10
2018-10	LANDSAT_8-B10	2018-12	LANDSAT_8-B10	2018-13	LANDSAT_8-B10
2019-29	LANDSAT_8-B10	2019-15	LANDSAT_8-B10	2019-16	LANDSAT_8-B10

Thermal calibration parameters for Landsat 5-7-8 (K_1 and K_2 constants, gain, and bias) are given in Table 4 (Chander et al. 2009).

After the effective at-sensor brightness temperature (T) was calculated, the SST pixel values were extracted from 1326 grids for the summer season of each year. Finally, the extracted pixel values were compared by using statistical methods with metrics such as the minimum, maximum, average, and standard deviation.

Validation An ideal way for validation may be obtaining the in situ SST data at the same time with the pass of the Landsat satellite. However, in this study, due to no in situ data available, we have used the Mediterranean Sea Ultra High Resolution (MSUHR) SST L4 Analysis 0.01 deg Resolution data as a reference for validation (Xing et al. 2006). MSUHR data has been produced by Group for High-Resolution Sea Surface Temperature (GHRSST) Level 4 AVHRR_OI Global Blended Sea Surface

Table 2 Day difference between images of the same month in different years. Among the available satellite images, it has been chosen to minimize the difference in days between the images of the same month in different years. For example, the day difference is 3 days for images between June 1990 and June 1989

June	Day differences	July	Day differences	August	Day differences
1989-10	Start	1989-28	Start	1989-13	Start
1990-13	3	1990-31	3	1990-08	5
1991-16	3	1991-18	13	1991-19	11
1992-18	2	1992-04	14	1992-21	8
1993-21	3	1993-23	19	1993-24	3
1994-24	3	1994-10	13	1994-11	13
1995-27	3	1995-13	3	1995-14	3
1996-29	2	1996-15	2	1996-16	2
1997-16	13	1997-02	13	1997-19	3
1998-19	3	1998-21	19	1998-06	13
1999-22	3	1999-24	3	1999-17	9
2000-24	2	2000-26	2	2000-19	2
2001-27	3	2001-05	21	2001-06	13
2002-30	3	2002-24	19	2002-09	3
2003	N/A	2003-03	19	2003-20	11
2004-03	17	2004-21	17	2004-22	2
2005-22	18	2005-24	3	2005-25	3
2006-09	11	2006-27	3	2006-28	3
2007-12	3	2007-30	3	2007-15	3
2008-30	18	2008	N/A	2008-17	2
2009-17	13	2009-19	11	2009-20	3
2010-04	13	2010-06	13	2010-23	3
2011-23	19	2011-09	3	2011-10	13
2012	N/A	2012	N/A	2012	N/A
2013-28	5	2013-30	21	2013-15	5
2014-15	13	2014-01	29	2014-18	3
2015-18	3	2015-20	19	2015-21	3
2016-20	2	2016-06	14	2016-07	14
2017-23	3	2017-09	3	2017-26	19
2018-10	13	2018-12	3	2018-13	13
2019-29	19	2019-15	3	2019-16	3
Average	8 days	Average	11 days	Average	7 days

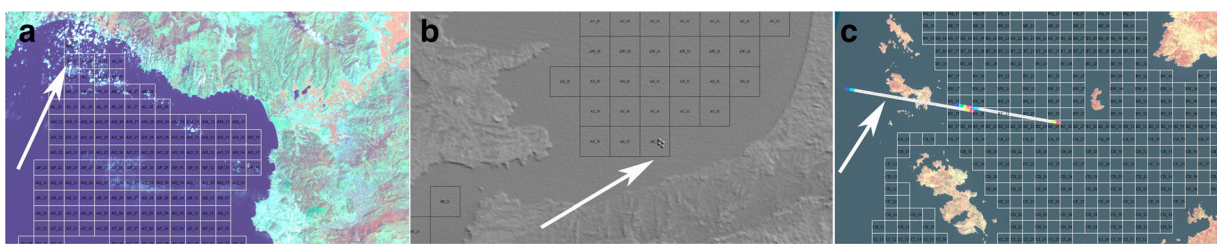

Fig. 2 Error types: cloud (**a**), unknown object (**b**), and sensor error (**c**)

Table 3 Missing grids for some years due to errors and cloud. The study area consists of 1326 grids, and each of grid is 2 km^2. For example, there are 75 missing grids in June 1989, which is 5.7% of the total area

Year	June - missing grid	July - missing grid	August - missing grid
1989	75 - Cloud (5.7%)	373 - Cloud (28.1%)	-
1990	19 - Error-B (1.4%)	-	-
1991	222 - Cloud (16.7%)	-	4 - Error-B (0.3%)
1992	148 - Cloud (11.2%)	-	86 - Error-C-Cloud (6.5%)
1993	-	-	17 - Error-C (1.3%)
1994	-	-	-
1995	-	18 - Cloud (1.4%)	-
1996	-	5 - Out of border (0.4%)	-
1997	-	-	-
1998	-	-	-
1999	100 - Cloud (7.5%)	-	-
2000	-	-	-
2001	-	-	-
2002	-	-	-
2003	N/A	-	-
2004	122 - Cloud (9.2%)	-	-
2005	-	-	-
2006	224 - Cloud (16.9%)	-	219 - Cloud (16.5%)
2007	-	-	-
2008	-	N/A	-
2009	-	-	-
2010	132 - Cloud (10.0%)	-	-
2011	-	-	-
2012	N/A	N/A	N/A
2013	-	-	-
2014	20 - Cloud (1.5%)	-	23 - Cloud (1.7%)
2015	-	-	-
2016	-	-	-
2017	-	-	-
2018	-	-	167 - Cloud (12.6%)
2019	-	-	-

Temperature Analysis, from the National Centers for Environmental Information (NCEI), available at the Physical Oceanography Distributed Active Archive Center (PODAAC) of the Jet Propulsion Laboratory from NASA (Nardelli et al. 2013). GHRSST is obtained by optimal interpolation from different data sources such as AVHRR satellite sensors and in situ data, with a 0.25-degree spatial resolution (Banzon et al. 2016; Pastor et al. 2017). We have extracted the dataset over the Aegean Sea during the 2008–2019 period as a reference for comparison because daily GHRSST-SST data is available from January 1, 2008, to the present, and is updated in near real-time. Then, for validation, regression analysis was conducted between GHRSST and Landsat data for the 2008–2019 period.

Results

In this research, spatial and temporal analysis of SST for summer seasons during the 30-year period has been carried

Table 4 Thermal calibration parameters for Landsat 5-7-8 (from metadata file of Landsat 8 and Chander et al. 2009)

Sensor	K_1(W/(m^2. sr. μm)	K_2 (K)	Gain	Bias
Landsat 5 TM	607.76	1260.56	0.055158	1.2378
Landsat 7 TM and ETM+	666.09	1282.71	0.037205	3.2
Landsat 8 TIRS-B10	77.488	1321.08	0.0003342	0.1000

out by using Landsat thermal infrared bands. Validation of the results was realized using GHRSST data. As a general result, the long-term trend of SST has been observed to increase, and a strong seasonal model has emerged. The detailed results were given in three categories as follows:

- monthly results for June, July, and August covering the summer period;
- results for the summer season of a 30-year period;
- validation-related results.

Monthly results for June, July, and August covering the summer period Seasonally, the highest average values of SST were found in August 2015 and the lowest in June 1992. The results of the analysis for June, July, and August covering the summer season are shown in Fig. 3 as a graphic.

As can be seen from Fig. 3, a continuous warming trend and a seasonal model has emerged. The top three lowest temperatures during the summer seasons for the 30-year period are the following: 1992, June with 15.53 ± 0.95; 2006, June with 15.87 ± 5.74; 2004, and June with 16.44 ± 1.63. The top three highest temperatures during the 30-year summer season are the following: 2015, August with 24.69 ± 0.56; 2001, August with 24.60 ± 0.84; 2018, and August with 24.25 ± 0.77. When looking at the satellite images with the highest SST and the lowest SST values during the summer seasons for the 30-year period, it was observed that while the southern and coastal regions have higher SST values, the northern and offshore regions have lower SST ones. In general, this result is an expected situation as SST values tend to increase as we descend to the south in the Northern Hemisphere (Fig. 4).

Results during the summer seasons for the 30-year period As described in the "Data and methods" section, all Landsat TIR images of the summer period are mapped as effective at-sensor brightness temperature. Average SST distribution maps during the summer seasons for the 30-year period are shown in Fig. 5. For a better understanding, the colour scale in the SST distribution map for each year was arranged according to the minimum and maximum values of that year. As shown in Fig. 5, the lowest average SST values were observed between Didim and the Gulf of Kusadasi, and the highest SST values in the Gulf of Gokova, Marmaris, and the Gulf of Gulluk. In the area between the Golf of Kusadasi and Didim, there is a large delta area where the Buyuk Menderes (Maiandros) River flows into the sea. The Buyuk Menderes River is the biggest river of Western Anatolia; it flows into the Aegean Sea and it is about 540 km in length. Therefore, because of the high amount of freshwater discharge into the sea during some periods, areas with low SST values can be seen in this region. These areas can especially be seen very clearly in the images from 1991, 1992, 1998, 2000, 2002, and 2007 as shown in Fig. 5.

All the minimum, maximum, and the average of summer season SST values by year are shown in Table 5. While SST values were low in the late 1980s and the early 1990s, SST values were found to be high in 2019. These values show that there is an upward trend in temperature. For example, it was calculated that the minimum value of the lowest SST was 17.75 °C; the minimum value of the highest SST was 18.99 °C; and the minimum value of the average SST was 18.44 ± 2.87 °C in 1992. However, the maximum value of the lowest SST was 23.18 °C in 2016; the maximum value of the highest SST was 23.76 °C in 2016; and the maximum value of the average SST was 23.45 ± 0.70 °C in 2018. These findings show us that a continuous warming trend might have happened for a part of the Aegean Sea for the 1989–2019 period. The findings also show us that the annual average SST value change was 0.11 °C. In this case, it can be said that the average SST change was 3.19 ± 1.26 °C for the entire 30-year period.

Validation-related results The regression analysis was conducted between GHRSST and Landsat data in the

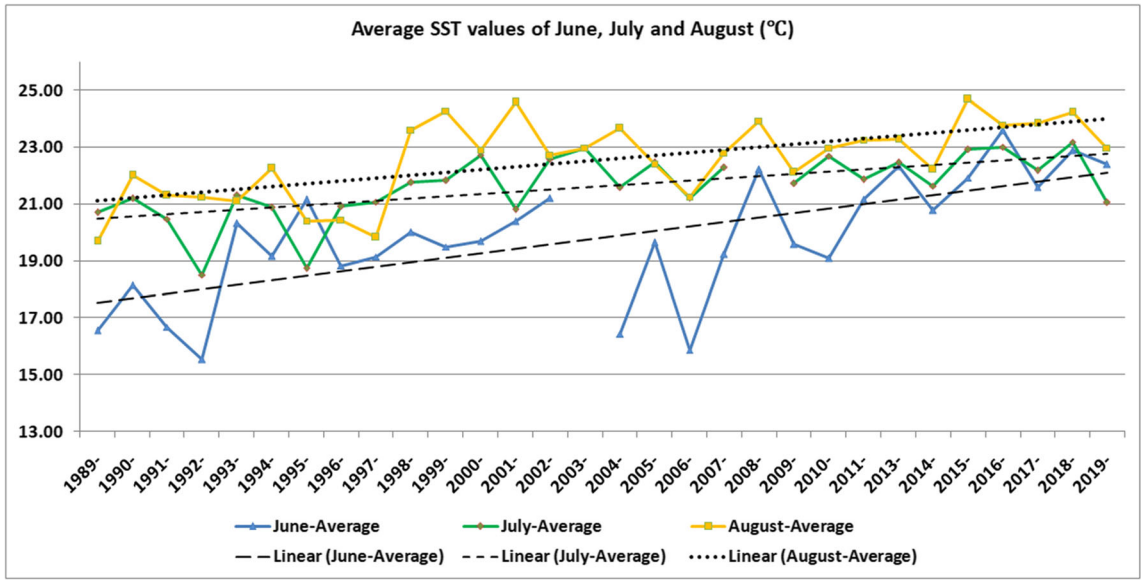

Fig. 3 Average SST values in °C for June, July, and August of the entire study area during a 30-year period

2008–2019 period for validation. The SST results between 2008 and 2019, from the two kinds of remote-sensing datasets, showed that there was a high linear correlation relationship between these years by month and season. Regression constant *R*-squared values were found to be 0.9672 for June, 0.9550 for July, 0.9634 for August, and 0.9634 for the summer seasons (Fig. 6a–d). Also, another interesting find, the 2008–2019 SST results, from the two kinds of remote-sensing datasets, showed that the SST results from Landsat were lower than those from GHRSST by 0.60 ± 0.20 °C (Fig. 6e). The reason for this small difference can be evaluated reasonably if it is taken into account that the time of the GHRSST's satellite overpass could be earlier or later than that of the Landsat, and also that there could exist resolution and sensor differences. However, as shown in Fig. 6e, it is clearly seen that there are increasing trends and a strong correlation in SST in both types of remote-sensing data.

Discussion

The purpose of the research and analysis in this study has been to determine whether there is any change in

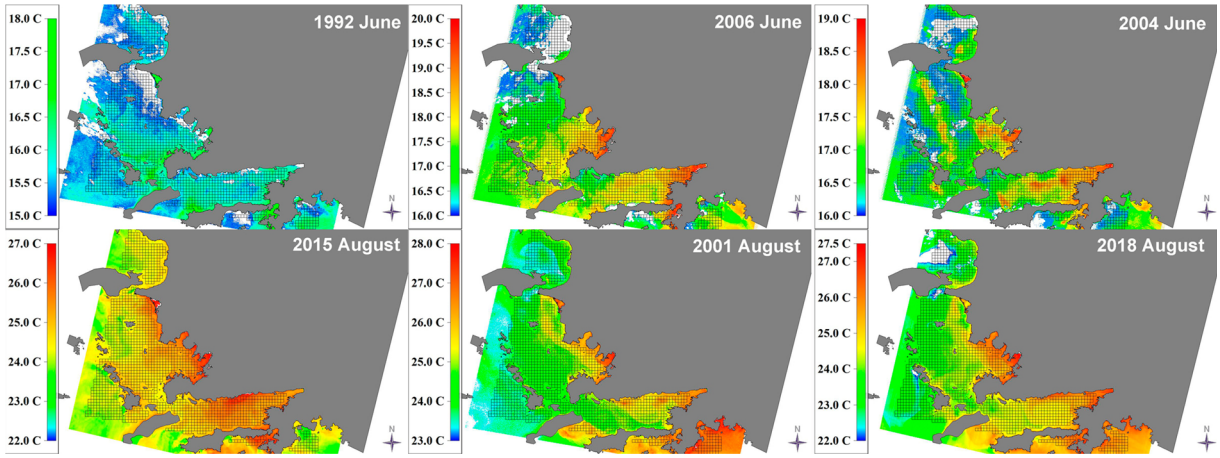

Fig. 4 The top three of the lowest (1992, 2006, and 2004 in June) and highest (2015, 2001, and 2018 in August) SST maps during the summer seasons for the 30-year period

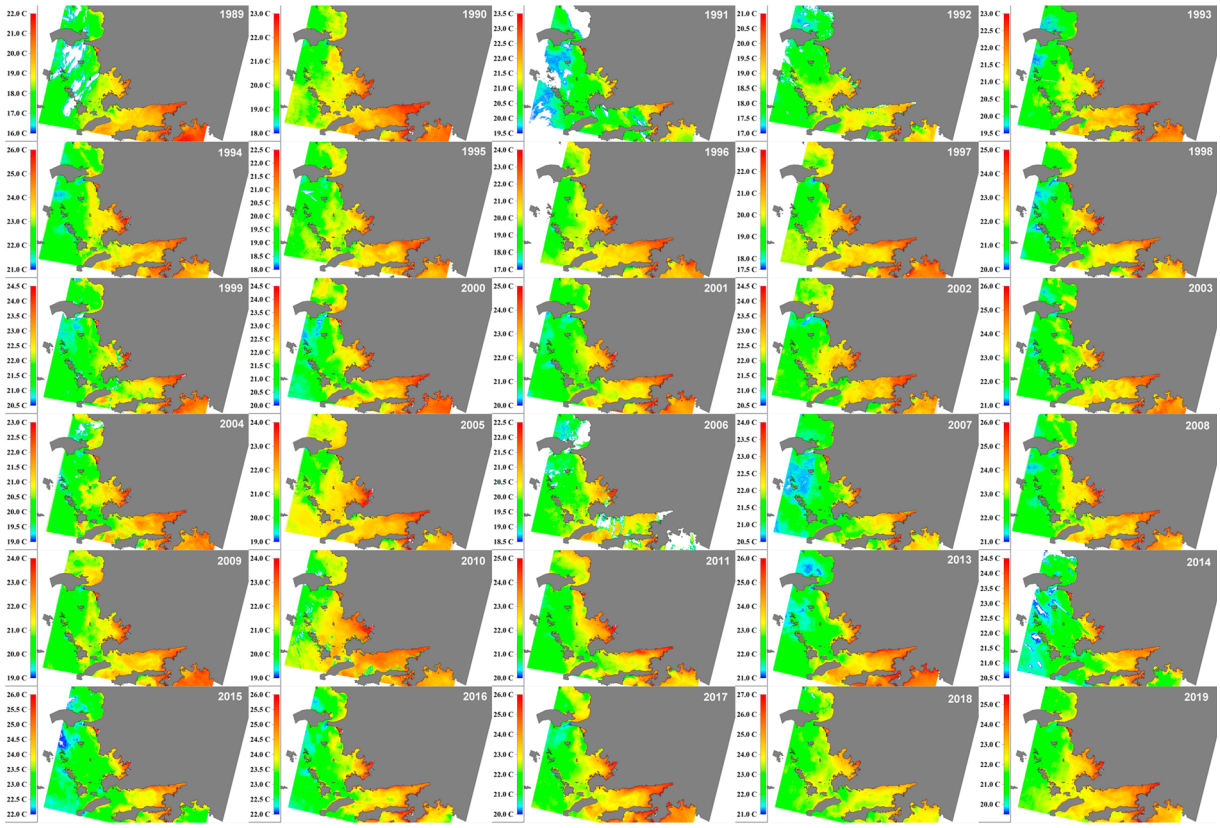

Fig. 5 (Minimum 16–maximum 27 °C) Average SST distribution maps for the summer seasons during the 30-year period. Average summer SST values were calculated by processing the SST images from June, July, and August in the raster calculator

SST in the research area for a 30-year period. A total of 88 Landsat 5, 7, and 8 TIR images were used in the months of June, July, and August for the analysis of SST changes during the summer seasons in the Aegean Sea. In order to validate the findings, regression analysis was performed between GHRSST and Landsat data for the 2008–2019 period. As a result of the analysis and the validation, it has been concluded that SST tends to increase in that part of the Aegean Sea, which also includes the research area. According to the Landsat data, over the past 30 years, from 1989 to 2019, it is estimated that the annual average SST changes were 0.11 °C, and the total changes of average STT were about + 3.19 ± 1.26 °C. The overall finding in this study shows that SST in the Aegean Sea has a rising trend. However, it is difficult to determine whether this upward trend is related to global climate change (Fig. 7).

Of course, this research has some limitations; because of missing images, there is no data from the area due to cloudiness, sensor errors, day differences between images, and validation by in situ data. However, these limitations are not considered to negatively affect the overall results of the analysis. Landsat images could not be found for all months in 2012. However, a single-year deficiency is not considered to affect the results much for a 30-year period. On the other hand, there are some day differences between satellite imagery dates. These differences are shown in Table 2. The average day temperature difference between Landsat images is 8 days for June, 11 days for July, and 7 days for August. Since the sea surface temperature will not change much in such a short time, it was thought that the day difference between the satellite images used in this research would not affect general results much.

Due to differences in satellite sensor and validation methods used to measure SST, there may be minor differences between the findings obtained in this study. We found a 0.60 ± 0.20 °C difference between GHRSST data used for validation and Landsat data. The gap of 0.60 °C can be evaluated reasonably if it is considered that the time of the GHRSST's satellite overpass could have been earlier or later than that of

Table 5 Minimum, maximum, average, and annual change value of SST as °C of the summer season (June-July-August) of the entire study area. Missing images of 2003-June, 2008-July, and 2012 are shown as (*). Only the 2003 summer season SST values have been calculated by July and August, and also for the 2008 summer season, SST values have been calculated by June and August

Summer Season (June-July-August) SST value (°C)					Change compared to the previous year average (°C)
No:	Year	Min	Max	Average	
1	1989	18.36	19.60	19.00	Start
2	1990	19.85	21.03	20.47	1.47
3	1991	18.21	20.50	19.50	− 0.97
4	1992	17.75	18.99	18.44	− 1.06
5	1993	20.21	21.63	20.92	2.48
6	1994	20.21	21.35	20.78	− 0.14
7	1995	19.59	20.65	20.11	− 0.67
8	1996	19.48	20.67	20.07	− 0.04
9	1997	19.49	20.58	20.03	− 0.04
10	1998	21.28	22.33	21.80	1.77
11	1999	21.16	22.50	21.88	0.08
12	2000	21.14	22.42	21.79	− 0.09
13	2001	21.19	22.68	21.94	0.15
14	2002	21.36	22.98	22.18	0.24
15	2003*	22.47	23.50	22.99	0.81
16	2004	19.87	21.19	20.57	− 2.42
17	2005	20.94	22.09	21.53	0.96
18	2006	18.50	20.18	19.45	− 2.08
19	2007	20.93	21.94	21.45	2.00
20	2008*	22.41	23.69	23.08	1.63
21	2009	20.63	21.70	21.15	− 1.93
22	2010	20.69	22.26	21.60	0.45
23	2011	21.56	22.63	22.11	0.51
24	2013	22.44	22.99	22.71	0.60
25	2012*	N/A	N/A	N/A	N/A
26	2014	21.12	21.91	21.56	− 1.15
27	2015	22.88	23.47	23.19	1.63
28	2016	23.18	23.76	23.48	0.29
29	2017	22.22	22.86	22.55	− 0.93
30	2018	23.13	23.75	23.45	0.90
31	2019	21.83	22.44	22.15	− 1.30
				Average annual change (°C)	0.11

the Landsat, there could exist resolution and sensor differences. However, as can be seen from Fig. 6e, it is clear that there are increasing trends and a strong correlation in SST in both types of remote-sensing data.

In this case, the general trend of SST measurement results based on satellite images can provide more realistic interpretations of SST variability. That is, if different remote-sensing data (satellite images) used in long-term observations, such as 30 years, show an increasing trend in SST, despite small differences in numerical values between them, a continuous warming trend can be assumed for the relevant region.

In this context, when the results of previous studies in the Aegean Sea and the Mediterranean are compared

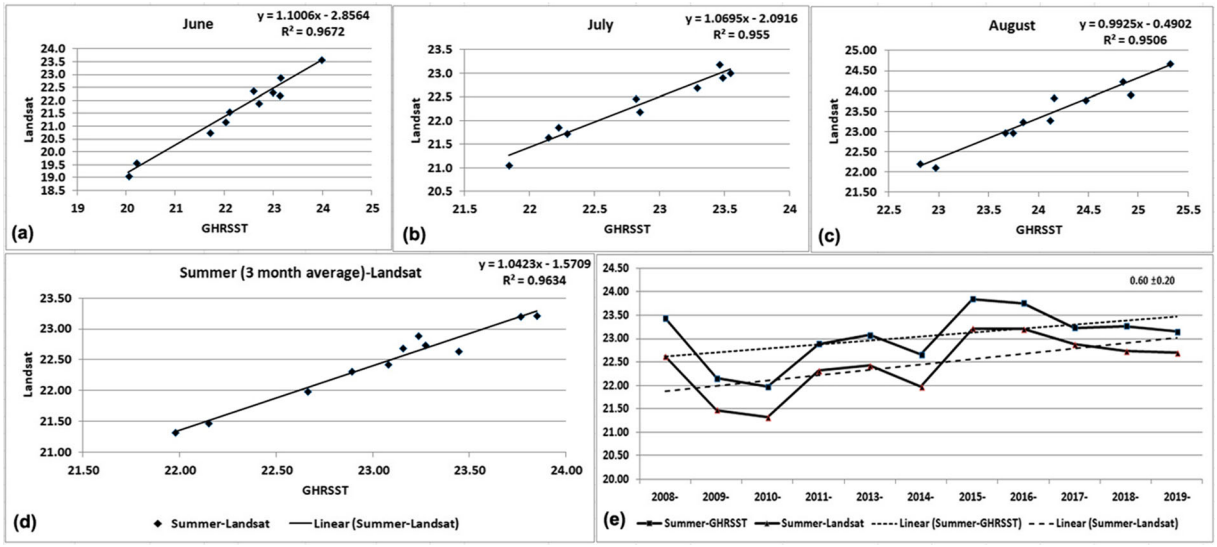

Fig. 6 Results of the regression analysis performed between GHRSST and Landsat data in the 2008–2019 period for validation. Regression constant *R*-squared values are as 0.9672 for June (**a**), 0.9550 for July (**b**), 0.9634 for August (**c**), and 0.9634 for the summer seasons (d). There is a 0.60 ± 0.20 °C gap between GHRSST and Landsat data (e)

with the findings and predictions in this research, it is seen that there are similar results and trends related to SST.

For instance, Pastor et al. (2017) found a consistent warming trend in a series of daily sea surface temperature data derived from satellites (1982–2016) for the whole Mediterranean region. Gucel and Sakalli (2018) investigated SST change in the Gulf of Iskenderun for the period of 1982–2015 by using remote-sensing data and found an SST change of approximately + 1.5 °C. Sakalli (2017) conducted a 30-year (1986–2015) SST analysis and found an increase of approximately 0.4 °C per decade, and in the last 30 years of this century (2071–2100), the relative increase in average SST in the Mediterranean was predicted by the model to be approximately 5.8 °C. Tsikliras et al. (2015) examined the effect of SST on the composition of catches in the Aegean Sea and the Ionian Sea for the periods of 1970–

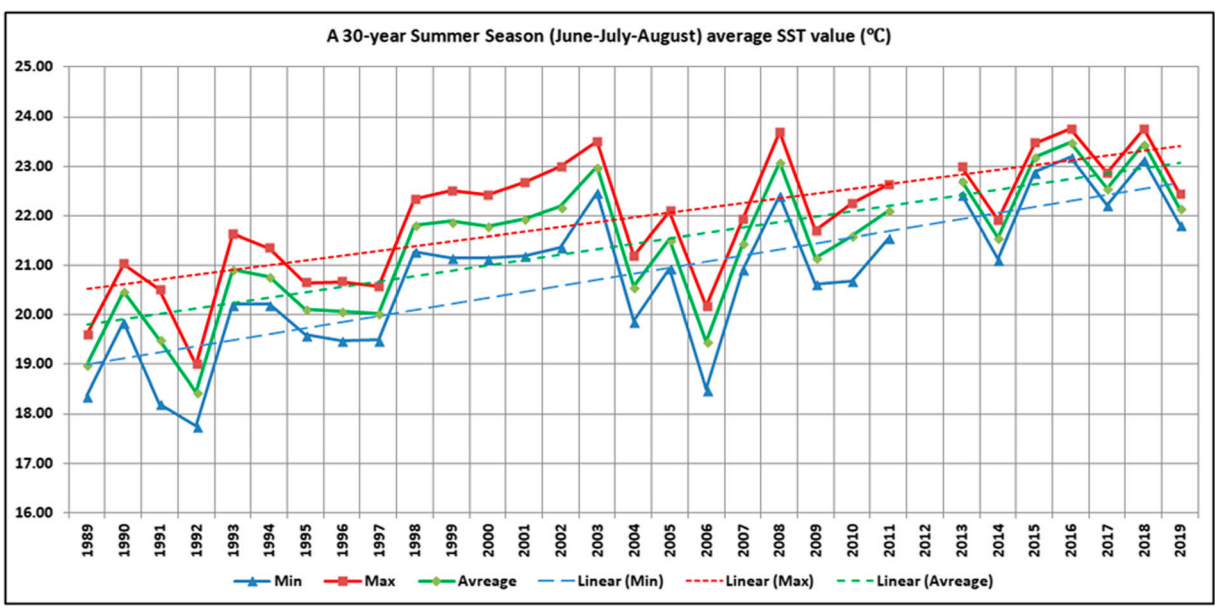

Fig. 7 Average SST values in °C during the summer seasons (June-July-August) for the 30-year period

2010 and 1997–2014 by using official catch statistics and bottom trawl survey data. According to their analyses, the rate of increase in the mean temperature of the catch (MTC) was 1.01 °C per decade in the Aegean Sea and 1.17 °C per decade in the Ionian Sea (Tsikliras et al. 2015). Skliris et al. (2011) investigated decadal-scale variability in Aegean Sea SST by using a long-term series of satellite and in situ data and constructed monthly mean SST maps for the 1985–2008 period. According to their results, the acceleration of surface warming in the Aegean Sea began to abruptly shift from strongly positive values to weakly positive/negative values. Topouzelis et al. (2012) investigated seasonal and monthly variations in SST in the Aegean Sea using MODIS images from 2005 to 2008 and found an increase in the minimum and maximum values of at least 1 °C.

Although this study does not cover the entire Aegean Sea or the Mediterranean Sea, its results are consistent with those from other studies on changes in SST. As it was seen in the abovementioned studies, also this study shows that the sea surface temperature has been increasing in the Aegean Sea for the 30-year period (1989 to 2019). However, it may be difficult to predict an exact increase or explain what factors drive it by looking merely at the result of this study. Although it is not possible to compare results obtained in this study in different scales, from different time periods and with different methods, these may be useful in establishing the general trends in SST.

References

Banzon, V., Smith, T. M., Chin, T. M., Liu, C., & Hankins, W. (2016). A long-term record of blended satellite and in situ sea-surface temperature for climate monitoring, modeling and environmental studies. *Earth System Science Data, 8*, 165–176. https://doi.org/10.5194/essd-8-165-2016.

Bertram, D. F., Mackas, D. L., & McKinnell, S. M. (2001). The seasonal cycle revisited: interannual variation and ecosystem consequences. *Progress in Oceanography., 49*, 283–307.

Bozkurt, D., & Sen, O. (2011). Precipitation in the Anatolian Peninsula: sensitivity to increased SSTs in the surrounding seas. *Climate Dynamics, 36*, 711–726. https://doi.org/10.1007/s00382-009-0651-3.

Brando, V. E., Braga, F., Zaggia, L., Giardino, C., Bresciani, M., Matta, E., Bellafiore, D., Ferrarin, C., Maicu, F., Benetazzo, A., Bonaldo, D., Falcieri, F. M., Coluccelli, A., Russo, A., & Carniel, S. (2015). High-resolution satellite turbidity and sea surface temperature observations of river plume interactions during a significant flood event. *Ocean Science, 11*, 909–920.

Chander, G., Markham, B. L., & Barsi, J. A. (2007). Revised Landsat-5 thematic mapper radiometric calibration. *IEEE Geoscience and Remote Sensing Letters., 4*(3), 490–494.

Chander, G., Markham, B. L., & Helder, D. L. (2009). Summary of current radiometric calibration coefficients for Landsat MSS, TM, ETM+, and EO-1 ALI sensors. *Remote sensing of environment, 113*, 893–903.

Costello, M. J., Smith, M., & Fraczek, W. (2015). Correction to surface area and the seabed area, volume, depth, slope, and topographic variation for the World's seas, oceans, and countries. *Environmental Science and Technology., 49*, 7071–7072.

Fisher, J. I., & Mustard, J. F. (2004). High spatial resolution sea surface climatology from Landsat thermal infrared data. *Remote Sensing of Environment, 90*, 293–307.

Gentemann, C. L., Wentz, F. J., Mears, C. A., & Smith, D. K. (2004). In situ validation of tropical rainfall measuring mission microwave sea surface temperatures. *Journal of Geophysical Research, 109*, C04021. https://doi.org/10.1029/2003JC002092.

Gucel, M. U., & Sakalli, A. (2018). Analysing sea surface temperature change in Gulf of Iskenderun from 1982 to 2015. *NESciences, 2018, 3*(2), 159–168.

Hansen, J., Ruedy, R., Sato, M., & Lo, K. (2010). Global surface temperature change. *Reviews of Geophysics, 48*, RG4004. https://doi.org/10.1029/2010RG000345.

Khalil, I., Atkinsona, P. M., & Challenorc, P. (2016). Looking back and looking forwards: Historical and future trends in seasurface temperature (SST) in the Indo-Pacific region from 1982 to 2100. *International Journal of Applied Earth Observation and Geoinformation, 45*, 14–26.

Laffoley, D., Baxter, J. M. (editors), (2016). Explaining ocean warming: causes, scale, effects and consequences. Full report. Gland: IUCN. 456 pp.

Luca, C., (2016). Semi-automatic classification plugin documentation. DOI: https://doi.org/10.13140/RG.2.2.29474.02242/1. 203p.

Nardelli, B.B., Tronconi, C,, Pisano, A., Santoleri, R., (2013). High and ultra-high resolution processing of satellite sea surface temperature data over southern European seas in the framework of MyOcean project. Remote Sens. Environ., *129*, 1-16, doi:10.1016 j.rse.2012.10.012.

Nikolakopoulos, G.K., Vaiopoulos, A.D., Skianis, G.A., (2003). Use of multitemporal remote sensing thermal data for the creation of temperature profile of Alfios River Basin. Conference: Geoscience and Remote Sensing Symposium, 2003. IGARSS '03. Proceedings. 2003 IEEE International.

Pastor, F., Valiente, J. A., & Palau, J. L. (2017). Sea surface temperature in the Mediterranean trends and spatial patterns (1982–2016). *Pure and Applied Geophysics, 175*, 4017–4029. https://doi.org/10.1007/s00024-017-1739-z.

Poulos, S. E., Drakopoulos, P. G., & Collins, M. B. (1997). Seasonal variability in sea surface oceanographic conditions in the Aegean Sea (Eastern Mediterranean): an overview. *Journal of Marine Systems, 13*, 225–244.

Ritchie, J.C., Cooper, C.M., (2001). Remote sensing techniques for determining water quality: application to TMDLs. In: TMDL Science Issues Conference, Water Environment Federation, Alexandria, VA. pp. 367–374.

Sakalli, A. (2017). Sea surface temperature change in the Mediterranean Sea under climate change: a linear model for simulation of the sea surface temperature up to 2100. *Applied Ecology and Environmental Research, 15*(1), 707–716.

Schmidt, G.A., Arndt, D., (2018). Annual Global analysis for 2017. News Conference January 2018, NOAA/NASA. 15p (https://www.giss.nasa.gov/research/news/20180118/NOAA-NASA_Global_Analysis-2017.pdf: accessed 15 April 2020).

Schott, J. R., Barsi, J. A., Nordgren, B. L., Raqueño, N. G., & Alwis, D. (2001). Calibration of Landsat thermal data and application to water resource studies. *Remote Sensing of Environment, 78*(1–2), 108–117.

Schott, J. R. (1982). An application of heat capacity mapping mission data: thermal bar studies of Lake Ontario. *Journal of Applied Photographic Engineering, 8*(3), 117–120.

Shaltout, M., & Anders Omstedt, A. (2014). Recent sea surface temperature trends and future scenarios for the Mediterranean Sea. *Oceanologia, 56*(3), 411–443.

Skliris, N., Sofianos, S. N., Gkanasos, A., Axaopoulos, A., Mantziafou, A., & Vervatis, V. (2011). Long-term sea surface temperature variability in the Aegean Sea. *Advances in Oceanography and Limnology, 2*(2), 125–139.

Syariza, M.A., Jaelania, L.M., Subehie, L., Pamungkasb, A., Koenhardonoc, E.S., Sulisetyonod, A., (2015). Retrieval of sea surface temperature over Poteran Island water of Indonesia with Landsat 8 TIRS image: a preliminary algorithm. The International Archives of the Photogrammetry, Remote Sensing and Spatial Information Sciences, Volume XL-2/W4, 2015 Joint International Geoinformation Conference 2015, 28–30 October 2015, Kuala Lumpur, Malaysia.

Topouzelis, K., Varnava, S., Georgiou, A., (2012). Spatial and temporal mapping of SST in East Mediterranean (Aegean Sea) during 2005-2008. Conference: Geoscience and Remote Sensing Symposium, 2012. IGARSS '12. Proceedings. 2012 IEEE International. pp.2617–2620.

Tsikliras, A. C., Peristeraki, P., Tserpes, G., & Stergiou, K. I. (2015). Mean temperature of the catch (MTC) in the Greek Seas based on landings and survey data. *Frontiers in Marine Science, 2*, 23. https://doi.org/10.3389/fmars.2015.00023.

Turuncoglu, U. U. (2015). Identifying the sensitivity of precipitation of Anatolian peninsula to Mediterranean and Black Sea surface temperature. *Climate Dynamics., 44*, 1993–2015. https://doi.org/10.1007/s00382-014-2346-7.

USGS, (2016). Landsat 8 (L8) data users handbook version 2. Department of the Interior U.S. Geological Survey. 106p.

Uncles, R. J., & Stephens, J. A. (2001). The annual cycle of temperature in a temperate estuary and associated heat fluxes to the coastal zone. *Journal of Sea Research., 46*, 143–159.

Vlahakis, G. N., & Pollatou, R. S. (1993). Temporal variability and spatial distribution of sea surface temperatures in the Aegean Sea. *Theoretical Applied. Climatology., 47*, 15–23.

Xing, Q., Chen, C., & Shi, P. (2006). Method of integrating Landsat-5 and Landsat-7 data to retrieve sea surface temperature in coastal waters on the basis of local empirical algorithm. *Ocean Science Journal, 41*(2), 97–104.